THE AMERICAN SOCIETY OF MECHANICAL ENGINEERS
345 E. 47th St., New York, N.Y. 10017

98-GT-484

REDUCED ORDER MODELING AND VIBRATION ANALYSIS OF MISTUNED BLADED DISK ASSEMBLIES WITH SHROUDS

Ronnie Bladh
Graduate Student

Matthew P. Castanier
Assistant Research Scientist

Christophe Pierre
Professor

Department of Mechanical Engineering and Applied Mechanics
The University of Michigan
Ann Arbor, MI 48109-2125
USA

ABSTRACT

This paper presents important improvements and extensions to a computationally efficient reduced order modeling technique for the vibration analysis of mistuned bladed disks. In particular, this work shows how the existing modeling technique is readily extended to turbomachinery rotors with shrouded blades. The modeling technique employs a component mode synthesis approach to systematically generate a Reduced Order Model (ROM) using component modes calculated from a Finite Element Model (FEM) of the rotor. Based on the total number of degrees of freedom, the ROM is typically two or three orders of magnitude smaller than the FEM. This makes it feasible to predict the forced response statistics of mistuned bladed disks using Monte Carlo simulations. In this work, particular attention is devoted to the introduction of mistuning into the ROM of a shrouded assembly. Mistuning is modeled by projecting the mistuned natural frequencies of a single, cantilever blade with free shrouds onto the harmonic modes of the shrouded blade assembly. Thus, the necessary mistuning information may be measured by testing individual blades.

1. INTRODUCTION

Based on the nominal design, a bladed disk assembly is a rotationally periodic structure. If it is assumed that each sector is identical, then the theory of cyclic symmetry may be used to analyze the dynamics of the entire structure based on, say, a finite element model of one sector (Joseph, 1981; Elchuri *et al.*, 1984; Hitchings and Singh, 1987). In practice, however, there are small differences among the structural properties of individual blades – due to manufacturing tolerances, material deviations, and non-uniform operational wear. These small, random discrepancies, commonly referred to as mistuning, are unavoidable. Furthermore, mistuning destroys the cyclic symmetry of the bladed disk assembly, and it can drastically affect the vibratory behavior of the structure. In particular, certain mode shapes may become spatially localized. As a result, a blade may experience forced response amplitudes and stresses that are substantially larger than those predicted by a tuned analysis.

The effects of mistuning on blade vibrations have been documented by experiments, as well as by analyses of representative lumped parameter models using numerical, statistical, and perturbation methods (Wagner, 1967; Dye and Henry, 1969; Ewins, 1969; Ewins, 1973; El-Bayoumy and Srinivasan, 1975; Griffin and Hoosac, 1984; Wei and Pierre, 1988a and 1988b; Lin and Mignolet, 1997). See Srinivasan (1997) for a survey of the literature. More recently, there have been efforts to use component mode synthesis (Irretier, 1983; Zheng and Wang, 1985; Castanier *et al.*, 1997) and receptance techniques (Yang and Griffin, 1997) combined with finite element models in order to obtain more accurate models of mistuned bladed disks.

The studies by Castanier *et al.* (1997) and Yang and Griffin (1997) are notable because specially-tailored techniques were employed to obtain, in a systematic fashion, highly reduced order models from parent finite element models of bladed disks. In particular, significant order reduction was achieved by reducing the number of degrees of freedom (DOF) needed to connect the disk and blade components. Yang and Griffin treated the disk-blade interface as having only rigid body motion, which reduced the necessary DOF to six for each blade. However, this approximation did cause some loss in accuracy in frequency regions that feature disk-blade interaction. In (Castanier *et al.*, 1997), a novel component mode technique was developed to eliminate the so-called constraint modes.

The technique of Castanier *et al.* (1997) has been applied to the analysis of the forced response of mistuned bladed disks (Kruse and Pierre, 1996a), and it has been validated using a finite element model of an industrial rotor (Kruse and Pierre, 1996b). However, these investigations concentrated on unshrouded bladed disk assemblies. In this paper, the reduced order modeling technique is extended to turbomachinery rotors with shrouded blades. The tuned blade-shroud ring is modeled as a single, cyclic component structure. Thus, the limiting cases of full stick or full slip at the shroud interfaces may be treated. Mistuning is added by projecting the mistuned natural frequencies of a single blade onto the

Presented at the International Gas Turbine & Aeroengine Congress & Exhibition
Stockholm, Sweden — June 2–June 5, 1998
This paper has been accepted for publication in the Transactions of the ASME
Discussion of it will be accepted at ASME Headquarters until September 30, 1998

cyclic modes of the blade-shroud ring. For an example finite element model, using the case of full stick at the shroud connections, excellent correlation between finite element and ROM predictions of the free and forced response is demonstrated.

This paper is organized as follows. The reduced order modeling technique is presented in Section 2, including updates to the ROM matrices, and specific formulations pertinent to shrouded assemblies are derived. A fairly detailed derivation of the proposed method to model mistuned shrouded assemblies is also included. In Section 3, the technique is applied to the vibration analysis of a shrouded test case rotor. The results are validated by comparisons with finite element results. Concluding remarks are given in Section 4.

2. REDUCED ORDER MODELING TECHNIQUE

2.1 General Formulation of Reduced Order Model

It may be assumed that the disk (d) and blade (b) degrees of freedom are ordered in such a manner as to give the following partitioning of the assembled mass and stiffness matrices of the entire structure:

$$\mathbf{M} = \begin{bmatrix} \mathbf{M_d} & \mathbf{0} \\ \mathbf{0} & \mathbf{M_b} \end{bmatrix} \qquad \mathbf{K} = \begin{bmatrix} \mathbf{K_d} & \mathbf{0} \\ \mathbf{0} & \mathbf{K_b} \end{bmatrix} \tag{1}$$

The location of the disk-to-blade interface can be chosen completely arbitrarily. In practice, though, this choice may affect the accuracy of the approximate solutions.

Each sector is here treated as an isolated substructure and since all sectors are assumed identical, the non-zero matrix blocks will be block-diagonal:

$$\begin{aligned} \mathbf{M_d} &= \mathbf{I} \otimes \tilde{\mathbf{M}}_\mathbf{d} \qquad & \mathbf{M_b} &= \mathbf{I} \otimes \tilde{\mathbf{M}}_\mathbf{b} \\ \mathbf{K_d} &= \mathbf{I} \otimes \tilde{\mathbf{K}}_\mathbf{d} \qquad & \mathbf{K_b} &= \mathbf{I} \otimes \tilde{\mathbf{K}}_\mathbf{b} \end{aligned} \tag{2}$$

where $\mathbf{I}$ is an identity matrix, and the symbol $\otimes$ denotes the Kronecker product, which is defined in Appendix A. The "tilde" notation will be used throughout the following to indicate that a quantity refers to a single blade or disk sector. Note that this implies that all degrees of freedom associated with the boundaries between adjacent sectors will appear twice.

A key idea for this reduced order modeling technique (Castanier *et al.*, 1997) is to describe the motion of the bladed disk assembly using two particular sets of component modes. Figure 1 depicts the two fundamental component mode types for a greatly simplified finite element model of a bladed disk sector. The first set is comprised of disk-induced modes, which are the cyclic modes of the entire assembly where the attached blades are massless. In this case, the blade motion is a rigid-body motion plus elastic deformation due to the boundary motion. The blade portion of the disk-induced modes, i.e. the part belonging to the blade degrees of freedom, will be denoted $\mathbf{U^d}$, and the disk portion $\mathbf{V^d}$. The second mode set consists of the modes of a cantilever blade alone, which is clamped at the chosen disk-blade interface location. Note that for unshrouded blades, the modal matrix $\mathbf{U^b}$ for all N identical blades is block-diagonal and is assembled as $\mathbf{I} \otimes \tilde{\mathbf{u}}^\mathbf{b}$, where $\tilde{\mathbf{u}}^\mathbf{b}$ is the cantilever mode shapes of a single blade. For shrouded blades, however, this set of modes is also cyclic in nature, due to the presence of direct blade-to-blade structural coupling, and thus, the cyclic assembly modes will yield a full matrix $\mathbf{U^b}$.

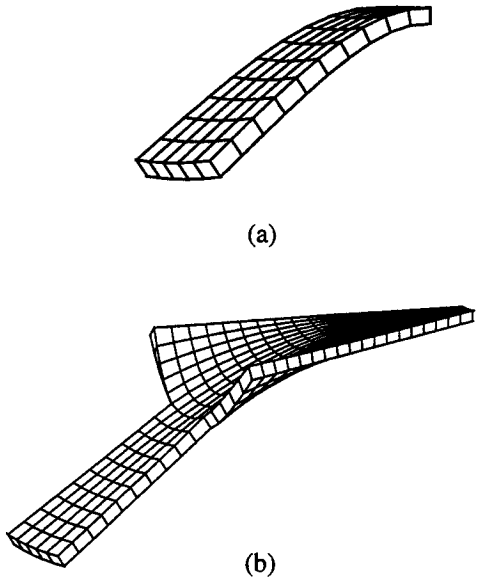

Fig. 1 Cantilever blade (a) and disk-induced (b) motions.

Through superposition of these two sets of component modes, and using the node ordering configuration in Eq. (1), the resulting nodal displacements of the entire assembly can be expanded as:

$$\mathbf{x} = \begin{bmatrix} \mathbf{V^d} \\ \mathbf{U^d} \end{bmatrix} \mathbf{a} + \begin{bmatrix} \mathbf{0} \\ \mathbf{U^b} \end{bmatrix} \mathbf{b} \tag{3}$$

where $\mathbf{a}$ and $\mathbf{b}$ are modal coordinates for the disk-induced and the cantilever blade modes, respectively. With above definitions, the strain and kinetic energies of the system, as well as the external virtual work done by a time-harmonic engine order excitation force, $\mathbf{Q}$, may be formulated in component modal-referred quantities.

Applying Hamilton's principle yields the governing equations of motion for the reduced order model. They are conveniently written in matrix form as:

$$\mathcal{M}\ddot{\mathbf{z}} + \mathcal{C}\dot{\mathbf{z}} + (1 + Gj)\,\mathcal{K}\mathbf{z} = \mathcal{Q} \tag{4}$$

where:

$$\mathbf{z} = \begin{Bmatrix} \mathbf{a} \\ \mathbf{b} \end{Bmatrix} \quad \mathcal{C} = \begin{bmatrix} \mathbf{0} & \mathbf{0} \\ \mathbf{0} & \mathbf{C} \end{bmatrix} \quad \mathcal{Q} = \begin{Bmatrix} \mathcal{Q}_\mathbf{d} \\ \mathcal{Q}_\mathbf{b} \end{Bmatrix} = \begin{Bmatrix} \mathbf{U^{d^T}Q} \\ \mathbf{U^{b^T}Q} \end{Bmatrix}$$

$$\mathcal{M} = \begin{bmatrix} \mathbf{I_d} + \mathbf{U^{d^T}M_bU^d} & \mathbf{U^{d^T}M_bU^b} \\ \mathbf{U^{b^T}M_bU^d} & \mathbf{I_b} \end{bmatrix}$$

$$\mathcal{K} = \begin{bmatrix} \hat{\mathbf{K}}_\mathbf{d} & \mathbf{U^{d^T}K_bU^b} \\ \mathbf{U^{b^T}K_bU^d} & \hat{\mathbf{K}}_\mathbf{b} + \Delta\hat{\mathbf{K}}_\mathbf{b} \end{bmatrix}$$

$\hat{\mathbf{K}}_\mathbf{d}$ and $\hat{\mathbf{K}}_\mathbf{b}$ are *diagonal* matrices, and the elements on the diagonals are modal stiffnesses (eigenvalues) obtained from the disk-induced and cantilever blade finite element analyses, respectively. $\mathbf{I_d}$ and $\mathbf{I_b}$ are the corresponding modal mass matrices, which in view of the employed method of eigenvector normalization will be identity matrices. Recall

that the blade is massless in the disk-induced analysis. Thus, the effect of blade mass on the disk is included as the second term in the upper-left quadrant of the mass matrix, but no such term is needed in the stiffness matrix.

Structural damping with damping coefficient G, as well as viscous modal damping of the cantilever blade modes, $\mathbf{C}$, have now been added to the reduced order model, in order to facilitate more realistic modeling of the structure's dynamic response. In addition, some general measure of mistuning, $\Delta\hat{\mathbf{K}}_\mathbf{b}$, is added into the stiffness matrix $\mathcal{K}$. This measure of mistuning, although general at this point, implies three assumptions:

- The mistuned characteristics of a blade are restricted to its stiffness (lower-right quadrant of $\mathcal{K}$). While stiffness mistuning is sufficient for the purposes of this study, it may be more accurate to model mistuning in other structural parameters as well; for instance, by using the mixed least squares – maximum likelihood method of Mignolet and Lin (1997).
- The effects of stiffness mistuning on the other three quadrants of $\mathcal{K}$ are assumed negligible. This is to a large extent justified by considering the kind of rigid-body-like motion the blade undergoes in this set of component modes.
- The mistuned cantilever modes of a blade may be realized by a linear combination of the tuned modes (i.e., they span approximately the same space).

Note that the resulting structural matrices are all symmetric. In general, this symmetry is destroyed if aerodynamic coupling between blades is introduced into the system. However, aerodynamic coupling will not be considered in this work.

At this point, the reduced order model formulation is completely general in that it is applicable to both unshrouded and shrouded assemblies. However, a closer examination of the various partitions of the structural matrices reveals significant differences between the two designs, leading to slightly different degrees of further simplifications. Further refinement of the formulation for unshrouded assemblies is detailed for the free response by Castanier *et al.* (1997), and extended for the forced response by Kruse and Pierre (1996a), and will therefore not be repeated here. A presentation of formulation details for the reduced order model of a shrouded assembly, including a novel method for modeling shrouded blade mistuning, will follow.

2.2 Formulation Refinement for Shrouded Designs

A modal matrix containing cyclic modes can be represented as:

$$\mathbf{U}^\mathbf{r} = (\mathbf{F} \otimes \mathbf{I})\,\tilde{\mathbf{U}}^\mathbf{r} \tag{5}$$

where $\mathbf{F}$ is defined in Eq. (B.3), and $\tilde{\mathbf{U}}^\mathbf{r}$, which contains the mode shapes of a fundamental sector in cyclic coordinates, has a *pseudo-block-diagonal* structure (see Appendix B):

$$\tilde{\mathbf{U}}^\mathbf{r} = \underset{k=0,\ldots,P}{\tilde{\mathbf{B}}\mathbf{diag}}\,[\tilde{\mathbf{u}}^\mathbf{r}_\mathbf{k}] \tag{6}$$

where $\tilde{\mathbf{B}}\mathbf{diag}\,[\bullet]$ denotes a pseudo-block-diagonal matrix, with the argument being the kth "block", and the range of k is shown. The mode type designation $\mathbf{r}$ could be either the disk-induced modes, $\mathbf{d}$, or the cantilever blade modes, $\mathbf{b}$, since the structure of both these modal matrices is cyclic. Combining Eqs. (5) and (6), one may write the internal structure of a cyclic modal matrix $\mathbf{U}^\mathbf{r}$ as:

$$\begin{aligned}\mathbf{U}^\mathbf{r} = \big[\ &\mathbf{f_0}\otimes\tilde{\mathbf{u}}^\mathbf{r}_\mathbf{0} \quad \mathbf{f_{1,c}}\otimes\tilde{\mathbf{u}}^\mathbf{r}_\mathbf{1,c} + \mathbf{f_{1,s}}\otimes\tilde{\mathbf{u}}^\mathbf{r}_\mathbf{1,s} \quad \cdots \\ &\cdots \quad \mathbf{f_{k,c}}\otimes\tilde{\mathbf{u}}^\mathbf{r}_\mathbf{k,c} + \mathbf{f_{k,s}}\otimes\tilde{\mathbf{u}}^\mathbf{r}_\mathbf{k,s} \quad \cdots \quad \mathbf{f_{N/2}}\otimes\tilde{\mathbf{u}}^\mathbf{r}_\mathbf{N/2}\ \big]\end{aligned} \tag{7}$$

Because of the cyclicity of both $\mathbf{U}^\mathbf{d}$ and $\mathbf{U}^\mathbf{b}$ and the block-diagonal structure of $\mathbf{M}$ and $\mathbf{K}$, all three projection products in $\mathcal{M}$ and $\mathcal{K}$ will become *pseudo-block-diagonal*:

$$\begin{aligned}\mathbf{U}^{\mathbf{d}^\mathbf{T}}\mathbf{M_b}\mathbf{U}^\mathbf{d} &= \underset{k=0,\ldots,P}{\tilde{\mathbf{B}}\mathbf{diag}}\left[\tilde{\mathbf{u}}^{\mathbf{d}^\mathbf{T}}_\mathbf{k}\tilde{\mathbf{M}}_\mathbf{b}\tilde{\mathbf{u}}^\mathbf{d}_\mathbf{k}\right] \\ \mathbf{U}^{\mathbf{d}^\mathbf{T}}\mathbf{M_b}\mathbf{U}^\mathbf{b} &= \underset{k=0,\ldots,P}{\tilde{\mathbf{B}}\mathbf{diag}}\left[\tilde{\mathbf{u}}^{\mathbf{d}^\mathbf{T}}_\mathbf{k}\tilde{\mathbf{M}}_\mathbf{b}\tilde{\mathbf{u}}^\mathbf{b}_\mathbf{k}\right] \\ \mathbf{U}^{\mathbf{d}^\mathbf{T}}\mathbf{K_b}\mathbf{U}^\mathbf{b} &= \underset{k=0,\ldots,P}{\tilde{\mathbf{B}}\mathbf{diag}}\left[\tilde{\mathbf{u}}^{\mathbf{d}^\mathbf{T}}_\mathbf{k}\tilde{\mathbf{K}}_\mathbf{b}\tilde{\mathbf{u}}^\mathbf{b}_\mathbf{k}\right]\end{aligned} \tag{8}$$

The external excitation force vector shown in Eq. (4), $\mathbf{Q}$, defines the forcing on all the blade degrees of freedom of the assembly. The restriction to blade degrees of freedom is not an absolute requirement, but leads to a more compact formulation, and it should also be sufficient from a practical perspective. Moreover, we assume an engine order excitation which is harmonic in time and differs only in phase from blade to blade. The phase at blade i, ϕ_i, is given by:

$$\phi_i = \frac{2\pi C(i-1)}{N} \qquad i = 1,\ldots,N \tag{9}$$

where C is the engine order of the excitation. The external force vector can then be expressed as:

$$\mathbf{Q} = \begin{Bmatrix} \tilde{\mathbf{f}}e^{j\phi_1} \\ \tilde{\mathbf{f}}e^{j\phi_2} \\ \vdots \\ \tilde{\mathbf{f}}e^{j\phi_N} \end{Bmatrix} \tag{10}$$

where $\tilde{\mathbf{f}}$ is the force vector on a single blade.

The expression for the modal force vector $\mathcal{Q}$ given in Eq. (4) can be simplified to a much more convenient form in terms of the disk-induced and cantilevered blade mode shapes of a single sector, $\tilde{\mathbf{u}}^\mathbf{d}_\mathbf{k}$ and $\tilde{\mathbf{u}}^\mathbf{b}_\mathbf{k}$, respectively. Using Eq. (10), and the modal matrix as written in Eq. (7), the corresponding modal force partition becomes:

$$\mathcal{Q}_\mathbf{r} = \mathbf{U}^{\mathbf{r}^\mathbf{T}}\mathbf{Q} = \sqrt{N}\begin{Bmatrix} \left(\mathbf{f_0}\otimes\tilde{\mathbf{u}}^\mathbf{r}_\mathbf{0}\right)^\mathbf{T}\left(\mathbf{e_C}\otimes\tilde{\mathbf{f}}\right) \\ \left(\mathbf{f_{1,c}}\otimes\tilde{\mathbf{u}}^\mathbf{r}_\mathbf{1,c} + \mathbf{f_{1,s}}\otimes\tilde{\mathbf{u}}^\mathbf{r}_\mathbf{1,s}\right)^\mathbf{T}\left(\mathbf{e_C}\otimes\tilde{\mathbf{f}}\right) \\ \vdots \\ \left(\mathbf{f_{k,c}}\otimes\tilde{\mathbf{u}}^\mathbf{r}_\mathbf{k,c} + \mathbf{f_{k,s}}\otimes\tilde{\mathbf{u}}^\mathbf{r}_\mathbf{k,s}\right)^\mathbf{T}\left(\mathbf{e_C}\otimes\tilde{\mathbf{f}}\right) \\ \vdots \\ \left(\mathbf{f_{N/2}}\otimes\tilde{\mathbf{u}}^\mathbf{r}_\mathbf{N/2}\right)^\mathbf{T}\left(\mathbf{e_C}\otimes\tilde{\mathbf{f}}\right) \end{Bmatrix} \tag{11}$$

where $\mathbf{e_C}$ is the $(C+1)$th column of the complex Fourier matrix, $\mathbf{E}$, defined in Eq. (B.2). This expression can now be greatly simplified, first by using the general algebraic properties of the Kronecker product stated in Eqs. (A.2) and (A.4), and then by making use of the orthogonal properties of the transformation column vectors involved. The expansion of Eq. (11) will yield modal force partitions that are zero everywhere, except for the Cth harmonic disk-induced and cantilever blade modes.

Thus, the engine order excitation, C, determines which modes of the assembly that are being excited. The resulting modal force vector is given in Section 2.4.

The modal viscous damping matrix for the shrouded cantilever blade modes, $\mathbf{C}$, will be a diagonal matrix expressed as:

$$\mathbf{C} = \underset{k=0,\ldots,P}{\tilde{\mathbf{B}}\mathbf{diag}} \left[\underset{n=1,\ldots,m_b/2m_b}{\mathbf{diag}} \left[2\zeta_n^k \right] \right] \sqrt{\hat{\mathbf{K}}_\mathbf{b}} \tag{12}$$

where $\mathbf{diag}\,[\bullet]$ denotes a diagonal matrix (block), with the argument being the nth diagonal element, and the range of n is shown. Also, ζ_n^k is the modal damping coefficient of the nth cantilever blade mode of the kth harmonic. Note that for shrouded blades, $\hat{\mathbf{K}}_\mathbf{b}$ is comprised of diagonal blocks associated with the various cyclic harmonics of the assembly of shrouded blades.

2.3 Mistuning of Shrouded Blades

Perhaps the most fundamental feature of this technique is its suitability for stiffness mistuning of the individual blades, since the modal stiffness of each individual cantilever blade mode is isolated in the diagonal matrix $\hat{\mathbf{K}}_\mathbf{b}$. Therefore, in the unshrouded case, the formulation lends itself to a very convenient and simple input of individual mistuning of each cantilever blade modal stiffness for each blade as:

$$\Delta\hat{\mathbf{K}}_\mathbf{b} = \underset{n=1,\ldots,N}{\mathbf{Bdiag}} \left[\underset{k=1,\ldots,m_b}{\mathbf{diag}} \left[\delta_n^k \right] \right] \hat{\mathbf{K}}_\mathbf{b} \tag{13}$$

where $\mathbf{Bdiag}\,[\bullet]$ denotes a block-diagonal (vs. pseudo-block-diagonal) matrix. The mistuning parameter associated with the kth cantilever blade mode of the nth blade, δ_n^k, is defined as:

$$\delta_n^k = \left(\frac{\bar{\omega}_n^k}{\omega^k} \right)^2 - 1 \tag{14}$$

where $\bar{\omega}_n^k$ represents the *mistuned* natural frequency of the kth mode of blade n, and ω^k is the corresponding nominal, or tuned, natural frequency.

However, the manner in which the mistuning is put into the ROM stiffness matrix for unshrouded blades is not particularly well suited for shrouded assemblies, in that $\hat{\mathbf{K}}_\mathbf{b}$ is now represented in *cyclic*, or *harmonic*, modal coordinates. This implies that in order to obtain any relevant measures of mistuning, one would need to know the effects of individual blade mistuning on the whole shrouded blade assembly. In theory, it would be possible to obtain this information through frequency tests of the full blade-shroud assembly, but this approach is not practical.

In view of this, an alternative approach is to project mistuning measurements for a single blade onto the cyclic modes of the blade assembly. In this case, the test data would consist of the deviations in natural frequencies of each individual mode of each blade. This data could then be used to generate estimates of the mistuned stiffness matrices for all blades, which would then be included in the ROM formulation. In addition, this would be possible to achieve without very complicated and specialized testing procedures.

First, one must establish the manner in which the individual shrouded blade natural frequencies are measured. Here, it is assumed that the shrouded blades are tested while being clamped at the root, but are otherwise completely unconstrained, as indicated in Fig. 2. Thus, the tests give measurements of the natural frequencies of a cantilever blade with free shrouds, $\bar{\omega}_n^k$. Using the mistuning parameter δ_n^k defined in Eq. (14),

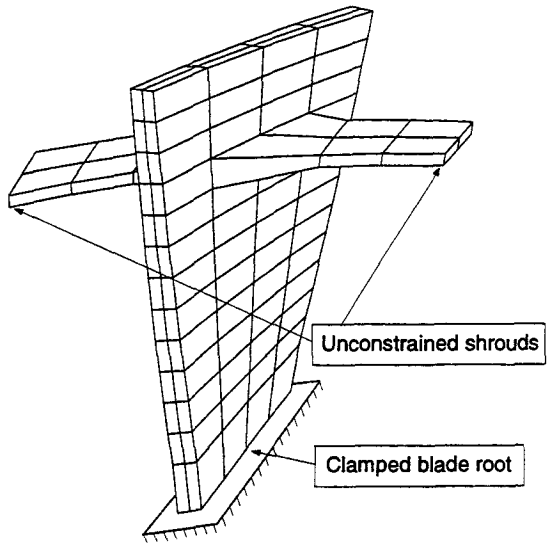

Fig. 2 Proposed configuration for measuring natural frequencies of shrouded blades individually.

a diagonal matrix containing the measured mistuned natural frequencies may be defined as:

$$\underset{n=1,\ldots,N}{\mathbf{Bdiag}} \left[\underset{k=1,\ldots,p}{\mathbf{diag}} \left[1 + \delta_n^k \right] \right] \hat{\mathbf{K}}_\mathbf{b}^{\mathbf{nom}} = \left(\mathbf{I} \otimes \bar{\mathbf{u}}^\mathbf{b} \right)^\mathbf{T} \mathbf{K}_\mathbf{b}^{\mathbf{mt}} \left(\mathbf{I} \otimes \bar{\mathbf{u}}^\mathbf{b} \right) \tag{15}$$

where $\bar{\mathbf{u}}^\mathbf{b}$ is the nominal modal matrix, or the nominal mode shapes, for one cantilever blade; $\mathbf{K}_\mathbf{b}^{\mathbf{mt}}$ is a mistuned, *block-diagonal* stiffness matrix, where each block corresponds to the stiffness matrix of one of the N mistuned blades; and $\hat{\mathbf{K}}_\mathbf{b}^{\mathbf{nom}}$ is a diagonal matrix of squared *nominal* natural frequencies for a tuned cantilever blade. The nominal natural frequencies may be taken either as some average values from tests, or directly from the finite element analysis needed to obtain the tuned cantilever blade mode shapes $\bar{\mathbf{u}}^\mathbf{b}$. Note that there is already an approximation made at this point, namely that the eigenvectors $\bar{\mathbf{u}}^\mathbf{b}$ of the mistuned blades are the same as the tuned ones (see discussion in Section 2.1).

Returning to Eq. (15), the mistuned frequencies are grouped in blocks associated with each individual blade, where these blocks are diagonal in themselves. Moreover, the mistuned stiffness matrix will have the following *block-diagonal* configuration:

$$\mathbf{K}_\mathbf{b}^{\mathbf{mt}} = \underset{n=1,\ldots,N}{\mathbf{Bdiag}} \left[\bar{\mathbf{K}}_{\mathbf{b},\mathbf{n}}^{\mathbf{mt}} \right] \tag{16}$$

Finally, the matrix of nominal modal stiffnesses will also be of a *block-diagonal* form, but where all the blocks are identical and diagonal. By denoting such a diagonal block $\hat{\bar{\mathbf{K}}}_\mathbf{b}^{\mathbf{nom}}$, the matrix of nominal modal stiffnesses can be expressed as:

$$\hat{\mathbf{K}}_\mathbf{b}^{\mathbf{nom}} = \underset{n=1,\ldots,N}{\mathbf{Bdiag}} \left[\hat{\bar{\mathbf{K}}}_\mathbf{b}^{\mathbf{nom}} \right] = \mathbf{I} \otimes \hat{\bar{\mathbf{K}}}_\mathbf{b}^{\mathbf{nom}} \tag{17}$$

Since $\hat{\bar{\mathbf{K}}}_\mathbf{b}^{\mathbf{nom}}$ represents the nominal modal stiffnesses for one blade, Eq. (17) can be rewritten as:

$$\hat{\mathbf{K}}_\mathbf{b}^{\mathbf{nom}} = \mathbf{I} \otimes \bar{\mathbf{u}}^{\mathbf{b}\mathbf{T}} \tilde{\mathbf{K}}_\mathbf{b} \bar{\mathbf{u}}^\mathbf{b} = \left(\mathbf{I} \otimes \bar{\mathbf{u}}^\mathbf{b} \right)^\mathbf{T} \left(\mathbf{I} \otimes \tilde{\mathbf{K}}_\mathbf{b} \right) \left(\mathbf{I} \otimes \bar{\mathbf{u}}^\mathbf{b} \right) \tag{18}$$

From Eqs. (15) and (18), one obtains:

$$\mathbf{K_b^{mt}} = \left(\mathbf{I}\otimes\bar{\mathbf{u}}^{\mathbf{b}}\right)^{\mathbf{T}^{-1}} \underset{n=1,\ldots,N}{\mathbf{Bdiag}}\left[\underset{k=1,\ldots,p}{\mathbf{diag}}\left[1+\delta_n^k\right]\right]\left(\mathbf{I}\otimes\bar{\mathbf{u}}^{\mathbf{b}^{\mathbf{T}}}\tilde{\mathbf{K}}_{\mathbf{b}}\right) \tag{19}$$

by virtue of the Kronecker product property given in Eq. (A.2).

Now, making use of the eigenvector normalization assumption, it is realized that:

$$\mathbf{I} = \underset{n=1,\ldots,N}{\mathbf{Bdiag}}\left[\bar{\mathbf{u}}^{\mathbf{b}^{\mathbf{T}}}\tilde{\mathbf{M}}_{\mathbf{b}}\bar{\mathbf{u}}^{\mathbf{b}}\right] = \left(\mathbf{I}\otimes\bar{\mathbf{u}}^{\mathbf{b}}\right)^{\mathbf{T}}\left(\mathbf{I}\otimes\tilde{\mathbf{M}}_{\mathbf{b}}\right)\left(\mathbf{I}\otimes\bar{\mathbf{u}}^{\mathbf{b}}\right)$$

$$\Rightarrow \quad \left(\mathbf{I}\otimes\bar{\mathbf{u}}^{\mathbf{b}}\right)^{\mathbf{T}^{-1}} = \mathbf{I}\otimes\tilde{\mathbf{M}}_{\mathbf{b}}\bar{\mathbf{u}}^{\mathbf{b}} \tag{20}$$

By substituting Eq. (20) into Eq. (19), and by using the fact that $\tilde{\mathbf{M}}_{\mathbf{b}}$ is symmetric, one may express the mistuned blade stiffness matrix as:

$$\mathbf{K_b^{mt}} = \mathbf{I}\otimes\tilde{\mathbf{K}}_{\mathbf{b}} + \left(\mathbf{I}\otimes\tilde{\mathbf{M}}_{\mathbf{b}}\bar{\mathbf{u}}^{\mathbf{b}}\right)\underset{n=1,\ldots,N}{\mathbf{Bdiag}}\left[\underset{k=1,\ldots,p}{\mathbf{diag}}\left[\delta_n^k\right]\right]\left(\mathbf{I}\otimes\bar{\mathbf{u}}^{\mathbf{b}^{\mathbf{T}}}\tilde{\mathbf{K}}_{\mathbf{b}}\right) \tag{21}$$

For convenience, the quantity $\Delta\mathbf{K_b}$ is introduced to denote the stiffness deviation matrix as:

$$\Delta\mathbf{K_b} = \left(\mathbf{I}\otimes\tilde{\mathbf{M}}_{\mathbf{b}}\bar{\mathbf{u}}^{\mathbf{b}}\right)\underset{n=1,\ldots,N}{\mathbf{Bdiag}}\left[\underset{k=1,\ldots,p}{\mathbf{diag}}\left[\delta_n^k\right]\right]\left(\mathbf{I}\otimes\bar{\mathbf{u}}^{\mathbf{b}^{\mathbf{T}}}\tilde{\mathbf{K}}_{\mathbf{b}}\right) \tag{22}$$

such that:

$$\mathbf{K_b^{mt}} = \mathbf{I}\otimes\tilde{\mathbf{K}}_{\mathbf{b}} + \Delta\mathbf{K_b} = \mathbf{K_b} + \Delta\mathbf{K_b} \tag{23}$$

The expression for the stiffness deviation matrix, $\Delta\mathbf{K_b}$, can be simplified to:

$$\Delta\mathbf{K_b} = \underset{n=1,\ldots,N}{\mathbf{Bdiag}}\left[\tilde{\mathbf{M}}_{\mathbf{b}}\bar{\mathbf{u}}^{\mathbf{b}}\underset{k=1,\ldots,p}{\mathbf{diag}}\left[\delta_n^k\right]\bar{\mathbf{u}}^{\mathbf{b}^{\mathbf{T}}}\tilde{\mathbf{K}}_{\mathbf{b}}\right] \tag{24}$$

Finally, the complete blade stiffness matrix for the tuned case, $\mathbf{K_b}$, is now simply replaced by $\mathbf{K_b^{mt}}$ in the reduced order model formulation. Thus, replacing $\mathbf{K_b}$ by $\mathbf{K_b^{mt}}$ in Eq. (1), and ignoring any contributions of mistuning from the projection onto the disk-induced modes, as per discussion in Section 2.1, yield the ROM stiffness matrix for a general mistuned shrouded bladed disk assembly:

$$\mathcal{K} = \begin{bmatrix} \hat{\mathbf{K}}_{\mathbf{d}} & \tilde{\mathbf{B}}\underset{k=0,\ldots,P}{\mathbf{diag}}\left[\tilde{\mathbf{u}}_{\mathbf{k}}^{\mathbf{d}^{\mathbf{T}}}\tilde{\mathbf{K}}_{\mathbf{b}}\tilde{\mathbf{u}}_{\mathbf{k}}^{\mathbf{b}}\right] \\ \tilde{\mathbf{B}}\underset{k=0,\ldots,P}{\mathbf{diag}}\left[\tilde{\mathbf{u}}_{\mathbf{k}}^{\mathbf{b}^{\mathbf{T}}}\tilde{\mathbf{K}}_{\mathbf{b}}\tilde{\mathbf{u}}_{\mathbf{k}}^{\mathbf{d}}\right] & \hat{\mathbf{K}}_{\mathbf{b}} + \mathbf{U}^{\mathbf{b}^{\mathbf{T}}}\Delta\mathbf{K_b}\mathbf{U}^{\mathbf{b}} \end{bmatrix}$$

$$\Delta\mathbf{K_b} = \underset{n=1,\ldots,N}{\mathbf{Bdiag}}\left[\tilde{\mathbf{M}}_{\mathbf{b}}\bar{\mathbf{u}}^{\mathbf{b}}\underset{k=1,\ldots,p}{\mathbf{diag}}\left[\delta_n^k\right]\bar{\mathbf{u}}^{\mathbf{b}^{\mathbf{T}}}\tilde{\mathbf{K}}_{\mathbf{b}}\right] \tag{25}$$

Thus, the stiffness mistuning $\Delta\mathbf{K_b}$, which may be obtained from measuring natural frequencies of individual blades with clamped roots and unconstrained shrouds, is now projected onto the cyclic modes of the shrouded blade assembly, $\mathbf{U^b}$. Note that the mistuning projection term $\mathbf{U}^{\mathbf{b}^{\mathbf{T}}}\Delta\mathbf{K_b}\mathbf{U}^{\mathbf{b}}$ does not yield any particular matrix structure, since there are no special relations, such as orthogonality, between the modes of the cantilever blade with unconstrained shrouds, and the cyclic modes of the shrouded blade assembly. Thus, in general, the lower-right quadrant of the ROM stiffness matrix becomes fully populated when mistuning is introduced for shrouded bladed disk assemblies.

2.4 Final Formulation for Shrouded Designs

To conclude this section, the reduced order model structural matrices (in the absence of aerodynamic coupling) and modal force for shrouded bladed disks are stated in their final forms:

$$\mathcal{M} = \begin{bmatrix} \mathbf{I_d} + \tilde{\mathbf{B}}\underset{k=0,\ldots,P}{\mathbf{diag}}\left[\tilde{\mathbf{u}}_{\mathbf{k}}^{\mathbf{d}^{\mathbf{T}}}\tilde{\mathbf{M}}_{\mathbf{b}}\tilde{\mathbf{u}}_{\mathbf{k}}^{\mathbf{d}}\right] & \tilde{\mathbf{B}}\underset{k=0,\ldots,P}{\mathbf{diag}}\left[\tilde{\mathbf{u}}_{\mathbf{k}}^{\mathbf{d}^{\mathbf{T}}}\tilde{\mathbf{M}}_{\mathbf{b}}\tilde{\mathbf{u}}_{\mathbf{k}}^{\mathbf{b}}\right] \\ \tilde{\mathbf{B}}\underset{k=0,\ldots,P}{\mathbf{diag}}\left[\tilde{\mathbf{u}}_{\mathbf{k}}^{\mathbf{b}^{\mathbf{T}}}\tilde{\mathbf{M}}_{\mathbf{b}}\tilde{\mathbf{u}}_{\mathbf{k}}^{\mathbf{d}}\right] & \mathbf{I_b} \end{bmatrix}$$

$$\mathcal{C} = \begin{bmatrix} \mathbf{0} & \mathbf{0} \\ \mathbf{0} & \underset{k=1,\ldots,m_b N}{\mathbf{diag}}\left[2\zeta^k\right]\sqrt{\hat{\mathbf{K}}_{\mathbf{b}}} \end{bmatrix}$$

$$\mathcal{K} = \begin{bmatrix} \hat{\mathbf{K}}_{\mathbf{d}} & \tilde{\mathbf{B}}\underset{k=0,\ldots,P}{\mathbf{diag}}\left[\tilde{\mathbf{u}}_{\mathbf{k}}^{\mathbf{d}^{\mathbf{T}}}\tilde{\mathbf{K}}_{\mathbf{b}}\tilde{\mathbf{u}}_{\mathbf{k}}^{\mathbf{b}}\right] \\ \tilde{\mathbf{B}}\underset{k=0,\ldots,P}{\mathbf{diag}}\left[\tilde{\mathbf{u}}_{\mathbf{k}}^{\mathbf{b}^{\mathbf{T}}}\tilde{\mathbf{K}}_{\mathbf{b}}\tilde{\mathbf{u}}_{\mathbf{k}}^{\mathbf{d}}\right] & \hat{\mathbf{K}}_{\mathbf{b}} + \mathbf{U}^{\mathbf{b}^{\mathbf{T}}}\Delta\mathbf{K_b}\mathbf{U}^{\mathbf{b}} \end{bmatrix}$$

$$\Delta\mathbf{K_b} = \underset{n=1,\ldots,N}{\mathbf{Bdiag}}\left[\tilde{\mathbf{M}}_{\mathbf{b}}\bar{\mathbf{u}}^{\mathbf{b}}\underset{k=1,\ldots,p}{\mathbf{diag}}\left[\delta_n^k\right]\bar{\mathbf{u}}^{\mathbf{b}^{\mathbf{T}}}\tilde{\mathbf{K}}_{\mathbf{b}}\right]$$

$$\mathcal{Q} = \begin{Bmatrix} \mathcal{Q}_{\mathbf{d}} \\ \mathcal{Q}_{\mathbf{b}} \end{Bmatrix} = \begin{Bmatrix} \mathbf{0} \\ \vdots \\ \mathbf{0} \\ \sqrt{N}\left\{\mathbf{f}_{\mathbf{C},\mathbf{c}}^{\mathbf{T}}\mathbf{e_C}\otimes\tilde{\mathbf{u}}_{\mathbf{C},\mathbf{c}}^{\mathbf{d}^{\mathbf{T}}}\tilde{\mathbf{f}} + \mathbf{f}_{\mathbf{C},\mathbf{s}}^{\mathbf{T}}\mathbf{e_C}\otimes\tilde{\mathbf{u}}_{\mathbf{C},\mathbf{s}}^{\mathbf{d}^{\mathbf{T}}}\tilde{\mathbf{f}}\right\} \\ \mathbf{0} \\ \vdots \\ \mathbf{0} \\ \hline \mathbf{0} \\ \vdots \\ \mathbf{0} \\ \sqrt{N}\left\{\mathbf{f}_{\mathbf{C},\mathbf{c}}^{\mathbf{T}}\mathbf{e_C}\otimes\tilde{\mathbf{u}}_{\mathbf{C},\mathbf{c}}^{\mathbf{b}^{\mathbf{T}}}\tilde{\mathbf{f}} + \mathbf{f}_{\mathbf{C},\mathbf{s}}^{\mathbf{T}}\mathbf{e_C}\otimes\tilde{\mathbf{u}}_{\mathbf{C},\mathbf{s}}^{\mathbf{b}^{\mathbf{T}}}\tilde{\mathbf{f}}\right\} \\ \mathbf{0} \\ \vdots \\ \mathbf{0} \end{Bmatrix}$$

3. ANALYSIS OF A SHROUDED TEST CASE ROTOR

3.1 Finite Element and Reduced Order Models

The finite element model of the test case rotor that is analyzed in this study is shown in Figs. 3 and 4. The rotor features 24 blades. Each blade has a base pitch of 30° (measured from the axial direction), and a uniform twist of an additional 30° over its length. The base radius is 212 mm, and the blade length is 68 mm. The rotor is fixed at the interfaces towards adjacent rotating blade stages. This is believed to provide a reasonable description of the dynamics of the bladed disk assembly. Moreover, the studied test case rotor features shrouds, which are arbitrarily positioned at 10/13 of the blade length.

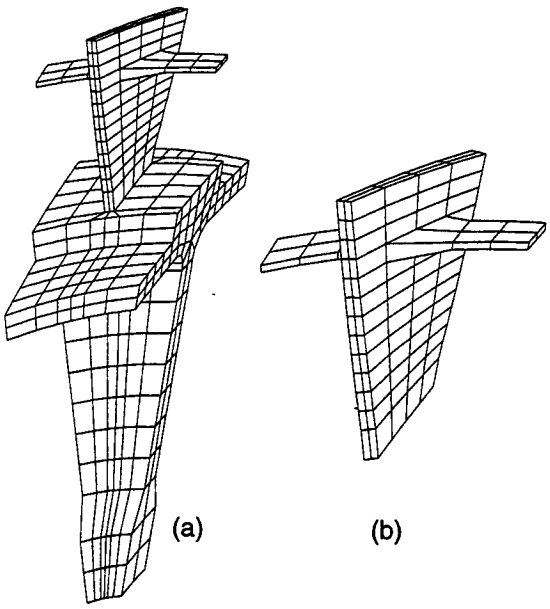

Fig. 3 (a) Finite element mesh of a single disk-blade-shroud sector. (b) Finite element mesh of a single blade with shrouds.

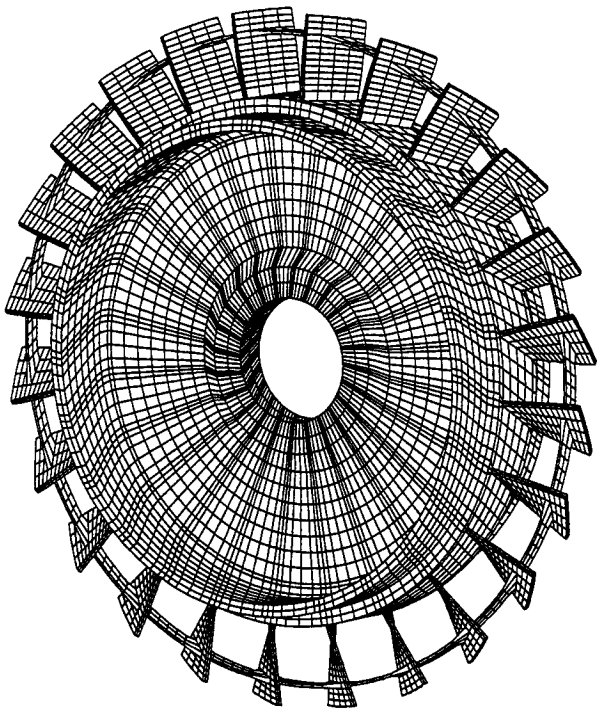

Fig. 4 Finite element mesh of full shrouded test case rotor.

The construction of the reduced order model of a shrouded assembly requires the following two finite element models:

- A complete sector subject to cyclic constraints at disk-to-disk and shroud-to-shroud interfaces. This model consists of 488 eight-noded brick elements and 2,646 degrees of freedom *before* model reduction due to applied constraints. The finite element mesh of this model is shown in Fig. 3a.
- A single cantilever blade. This model consists of 116 linear solid elements, and 738 degrees of freedom before model reduction. The finite element mesh of this model is shown in Fig. 3b.

From these fundamental finite element models, the reduced order model (ROM) is derived using the component mode synthesis technique described in Section 2. This analysis is based on a reduced order model that is created from five cantilever blade modes ($m_b = 5$) and five disk-induced modes ($m_d = 5$) per harmonic, leading to a total of 240 degrees of freedom.

In addition, five cantilever blade modes with unconstrained shrouds were used to generate the stiffness deviation matrix, $\Delta\mathbf{K_b}$ ($p = 5$). This, however, does not influence the size of the resulting reduced order model. It should be pointed out that, if the cantilever blade mode shapes from the cyclic symmetry analysis conform relatively closely with the cantilever blade mode shapes with unconstrained shrouds, very little improvement in accuracy is gained by including more than m_b modes for the stiffness deviation generation. In this case, the principal effects of the stiffness deviations are already captured by the m_b modes. However, using fewer than m_b modes yields poor accuracy and thus, in general, the condition $p \geq m_b$ should always be satisfied in order to obtain a reduced order model with reasonable accuracy.

Finally, a finite element model of the full mistuned rotor was created to allow comparisons of mistuned mode shapes and forced responses for a single, random mistuning pattern. The mistuning pattern was sampled from a uniform distribution of mean zero and standard deviation 5%. Individual mode mistuning is not employed in this analysis. Therefore, the mistuning is readily introduced to the full finite element model by appropriately varying Young's modulus in the blade elements as:

$$E_n = (1 + \delta_n)\, E_o \qquad n = 1, \ldots, N \tag{26}$$

The material properties for the finite element model were taken to be those of steel. The full finite element model consists of 11,712 linear solid elements and 56,376 degrees of freedom, and its finite element mesh is shown in Fig. 4.

It should be noted that the shroud-to-shroud connection is modeled as being continuous (full stick). Since no effort has been made to include friction at the shroud mating surfaces, the present modeling technique can be used for the limiting cases of full stick or full slip conditions. The incorporation of shroud interface models (Srinivasan *et al.*, 1978; Menq *et al.*, 1986; Valero and Bendiksen, 1986) into this type of reduced order model will be the subject of future work.

3.2 Free Vibration

Figure 5 displays the tuned natural frequencies versus the number of nodal diameters for the test case rotor in the lower frequency range, as obtained from finite element analysis and ROM analysis. MSC/NASTRAN^{TM} was used to calculate the natural frequencies and mode shapes of the finite element models, and to extract the blade mass and stiffness matrices ($\tilde{\mathbf{M}}_\mathbf{b}$ and $\tilde{\mathbf{K}}_\mathbf{b}$).

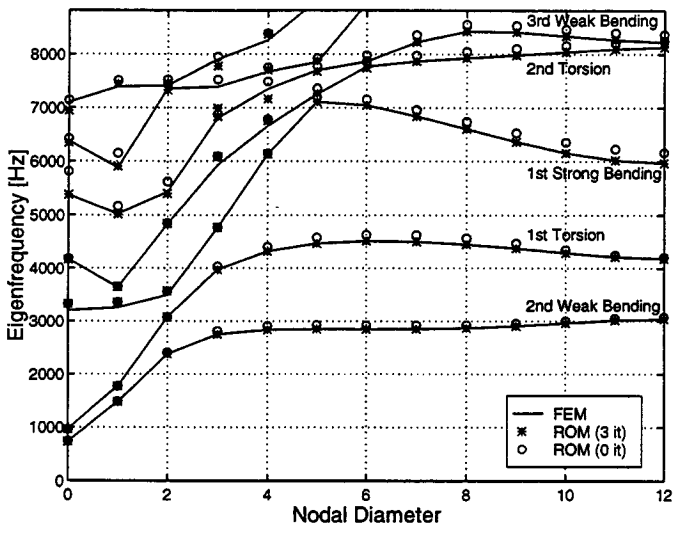

Fig. 5 Comparison of tuned eigenfrequencies from finite element model (FEM) and reduced order model (ROM) with and without eigenvalue adjustment iterations.

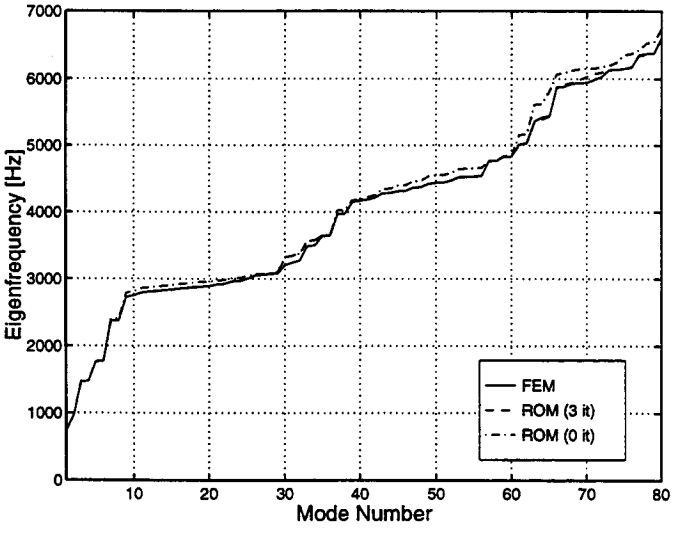

Fig. 6 Comparison of the 80 lowest mistuned eigenfrequencies from finite element model (FEM) and reduced order model (ROM) with and without eigenvalue adjustment iterations.

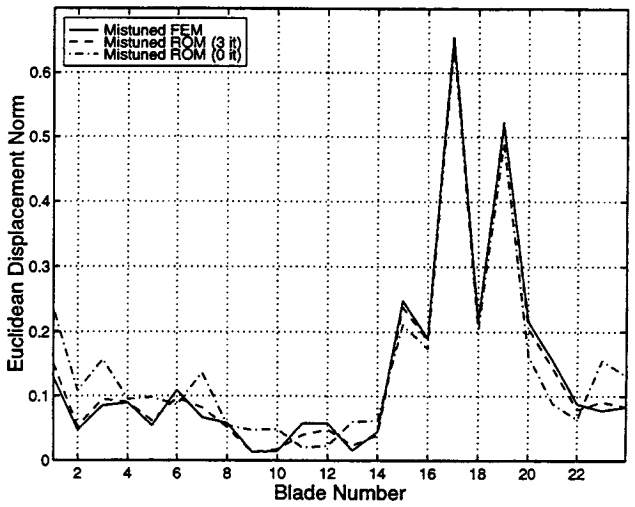

Fig. 7 Mistuned mode number 17 at 2861.7 Hz, as obtained by finite element model (FEM) and reduced order model (ROM) with and without eigenvalue adjustment iterations. This mode exhibits significant localization.

Clearly, as the number of nodal diameters increases, the disk becomes much more stiff. Thus, the slanted lines to the left in Fig. 5 correspond to disk-dominated modes. The lines which are approximately horizontal represent families of blade-dominated modes. The characteristic types of blade motion for the blade-dominated mode families are indicated in the plot. One can observe that, depending on the mode family, a slight stiffening or a slight softening occurs as the number of nodal diameters increase for the blade-dominated modes. This is somewhat different from the unshrouded case, where the frequencies associated with a certain family of blade-dominated modes are nearly constant over a certain range of nodal diameters.

Figure 5 also depicts the increase in ROM accuracy via eigenvalue adjustment. By directly adjusting the eigenvalues, or modal stiffnesses, associated with the blade modes (i.e., the diagonal elements of $\hat{\mathbf{K}}_b$), the ROM's representation of the blade-dominated modes is enhanced.

The adjustment procedure is a simple iterative process, where the cantilever blade eigenvalues are re-scaled based on the ratio between the tuned finite element eigenvalues from a cyclic symmetry analysis of a complete sector and the corresponding ROM eigenvalues. Once a sufficiently small residual is achieved, one may move on and introduce mistuning. As seen in Fig. 5, after three iterations of eigenvalue adjustments, the blade-mode frequencies for the ROM are nearly identical to those of the FEM. Naturally, the adjustments of the cantilever blade mode eigenvalues have a much smaller effect on the disk-dominated modes.

Figure 6 illustrates the correlation between finite element and ROM natural frequencies for the mistuned rotor. Since the nodal diameter description of the modes fails for certain mistuned modes due to localization, the natural frequencies are instead plotted versus the mode number in the mistuned case. Again, the results obtained from the reduced order model after eigenvalue adjustments compare very well with the finite element results.

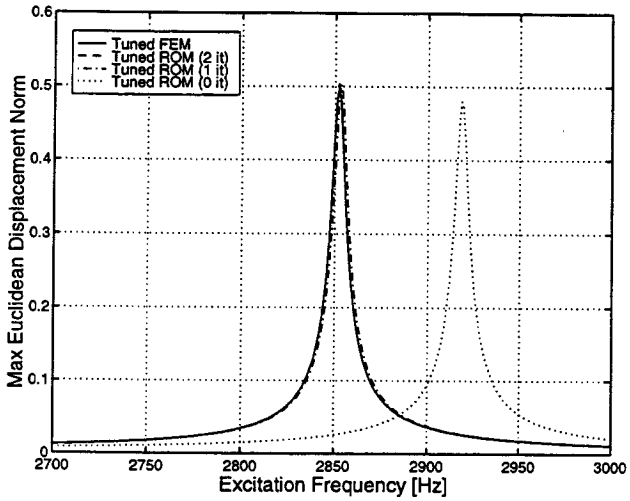

Fig. 8 Tuned forced response for engine order 7 excitation, as obtained by finite element model (FEM) and reduced order model (ROM) with and without eigenvalue adjustment iterations.

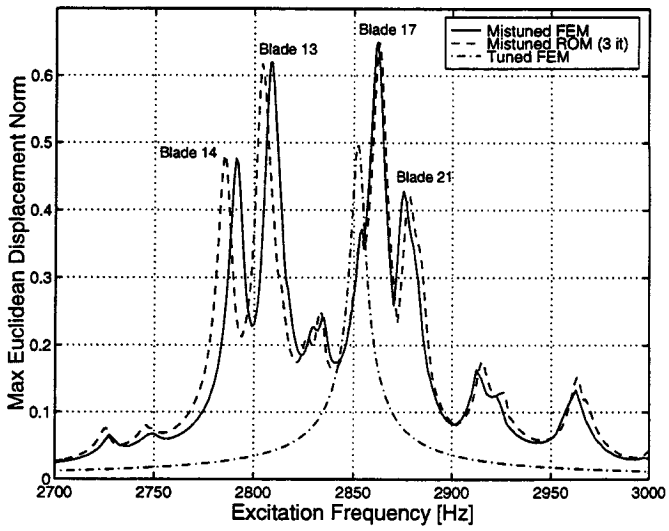

Fig. 9 Forced response for engine order 7 excitation, for both tuned and mistuned rotor, as obtained by finite element model (FEM) and reduced order model (ROM) with three eigenvalue adjustment iterations. The mistuned FEM has 56,376 degrees of freedom, while the ROM has only 240 degrees of freedom.

Figure 7 illustrates the correlation between finite element and ROM mistuned mode shapes. The Euclidean norm displacement measure, $\bar{u}_i$, for each blade i, is defined as:

$$\bar{u}_i = \left[\frac{\sum_{j=1}^{N_n} \left(u_{ij,r}^2 + u_{ij,\theta}^2 + u_{ij,z}^2 \right)}{\sum_{i=1}^{N_b} \sum_{j=1}^{N_n} \left(u_{ij,r}^2 + u_{ij,\theta}^2 + u_{ij,z}^2 \right)} \right]^{\frac{1}{2}} \tag{27}$$

where $u_{ij,x}$ is the displacement component in the x-direction, N_n is the number of nodes in one blade, and N_b is the total number of blades. The Euclidean norm is a scalar value, which may be interpreted as a measure of relative blade energy content.

Specifically, Fig. 7 shows the 17th mistuned mode at 2862 Hz, in which the vibration energy is largely confined to blades 17 and 19. The dramatic mode localization exhibited by this mode is due to the high modal density in this particular frequency region (Pierre, 1988). In fact, it is virtually impossible to find any traces of the corresponding smooth harmonic tuned shape from which it derives.

Note the excellent agreement between the FEM and the ROM mode shapes, especially after eigenvalue adjustment. Several important factors are extremely well captured, such as peak amplitude, position of localization, and rate of spatial decay away from the localized area.

3.3 Forced Response

Next, we consider the forced response of the blisk. The external excitation force consists of a unit nodal load applied on the tip of the blade's leading edge in the axial direction. This applied force was chosen arbitrarily, and it serves only to verify the accuracy of the reduced order model. Furthermore, the structure is excited according to engine order 7 excitation, which has a blade-to-blade forcing phase shift of 105°.

The tuned rotor's response to this external forcing is shown in Fig. 8. After only two iterations of eigenvalue adjustments, the FEM and ROM predictions of the tuned rotor's response are nearly identical. The difference between the resonant frequencies of the FEM and the ROM is reduced from 2.3% to 0.0007% after these two iterations. Also, the error in peak response amplitude decreases from −3.9% to 0.9%. This amplitude error did not improve during subsequent iterations.

Figure 9 shows the response of the mistuned rotor for the same source of excitation. The mistuning and localization effects lead to a substantial increase in peak response amplitude and, in addition, a very significant widening of the resonant frequency bandwidth, compared to the corresponding response of a tuned rotor. In absolute normed displacement values, the maximum resonance amplitude predicted by the ROM is less than 0.2% lower than that predicted by the FEM (0.649 versus 0.650), which is an acceptable discrepancy, considering the huge difference in model sizes.

A notable effect of the order reduction is that the reduced order model here predicts a somewhat wider band of resonant frequencies, compared to the finite element analysis, due to residual errors in the ROM mistuned eigenfrequencies. The ROM mistuned eigenfrequency of the 12th mode is 0.16% lower than the corresponding FEM frequency, while the approximation of the 17th mode eigenfrequency is 0.04% higher. The conformity of the response characteristics predicted by the reduced order model is otherwise reasonably accurate.

4. CONCLUSIONS

This paper demonstrates how the vibratory behavior of a mistuned bladed disk of a general design may be analyzed by a systematic and computationally efficient reduced order modeling technique, based on a component mode approach. In particular, this work showed how the technique could be extended to designs with shrouded blades, and how a convenient measure of individual blade mistuning may be incorporated

into the analysis with relative ease. Stiffness mistuning was included by projecting the mistuned natural frequencies of individual blades (with clamped roots and free shrouds) onto the cyclic modes of the shrouded blade assembly.

The reduced order modeling technique and the proposed method of mistuning for shrouded blade assemblies were validated using a finite element model (FEM) of a test case rotor. The total number of degrees of freedom for this FEM was 56,376, compared to only 240 for the reduced order model (ROM). The free and forced response results obtained for the ROM were in excellent agreement with those of the much larger FEM. Of special importance was the agreement of the forced response amplitudes for a rotor with mistuned blades. These results show that this reduced order modeling technique may provide a valuable tool for predicting the statistics of forced response for mistuned bladed disks.

ACKNOWLEDGEMENTS

This work is supported by the GUIde Consortium on blade durability at Carnegie Mellon University.

The authors would like to acknowledge the beneficial discussions of mistuning and reduced order modeling that they have had with the Director of the GUIde Consortium, Prof. J. H. Griffin.

REFERENCES

Castanier, M. P., Óttarsson, G., and Pierre, C., 1997, "A Reduced-Order Modeling Technique for Mistuned Bladed Disks," *Journal of Vibration and Acoustics*, Vol. 119, No. 3, pp. 439–447.

Davis, P. J., 1979, *"Circulant Matrices"*, Wiley-Intersciences.

Dye, R. C. F. and Henry, T. A., 1969, "Vibration Amplitudes of Compressor Blades Resulting From Scatter in Blade Natural Frequencies," *ASME Journal of Engineering for Power*, Vol. 91, No. 3, pp. 182–188.

El-Bayoumy, L. E. and Srinivasan, A. V., 1975, "Influence of Mistuning on Rotor-Blade Vibrations," *AIAA Journal*, Vol. 13, No. 4, pp. 460–464.

Elchuri, V., Smith, G. C. C., and Gallo, A. M., 1984, "NASTRAN Forced Vibration Analysis of Rotating Cyclic Structures," *ASME Journal of Vibration, Acoustics, Stress, and Reliability in Design*, Vol. 106, pp. 224–234.

Ewins, D. J., 1969, "The Effects of Detuning Upon the Forced Vibrations of Bladed Disks," *Journal of Sound and Vibration*, Vol. 9, No. 1, pp. 65–79.

Ewins, D. J., 1973, "Vibration Characteristics of Bladed Disc Assemblies," *Journal Mechanical Engineering Science*, Vol. 15, No. 3, pp. 165–186.

Griffin, J. H. and Hoosac, T. M., 1984, "Model Development and Statistical Investigation of Turbine Blade Mistuning," *ASME Journal of Vibration, Acoustics, Stress, and Reliability in Design*, Vol. 106, pp. 204–210.

Hitchings, D. and Singh, M., 1987, "Cyclic Symmetry Through Constraint Equations with Application to the Analysis of Steam Turbines," in *Bladed Disk Assemblies, Proceedings of the ASME 11th Biennial Conference on Mechanical Vibration and Noise,* Boston, Massachusetts, pp. 113–119.

Irretier, H., 1983, "Spectral Analysis of Mistuned Bladed Disk Assemblies by Component Mode Synthesis," in *Vibrations of Bladed Disk Assemblies, Proceedings of the ASME 9th Biennial Conference on Mechanical Vibration and Noise,* Dearborn, Michigan, pp. 115–125.

Joseph, J. A., 1981, "Cyclic Symmetry in MSC/NASTRAN," *MSC/NASTRAN Application Manual*, chapter 3.2, pp. 10–24, The MacNeal-Schwendler Corporation.

Kruse, M. J. and Pierre, C., 1996a, "Forced Response of Mistuned Bladed Disks Using Reduced-Order Modeling," *Proceedings of the 37th AIAA/ASME Structures, Structural Dynamics, and Materials Conference,* Salt Lake City, Utah.

Kruse, M. J. and Pierre, C., 1996b, "Dynamic Response of an Industrial Turbomachinery Rotor," *Proceedings of the 32nd AIAA/ASME/SAE/ASEE Joint Propulsion Conference and Exhibit,* Lake Buena Vista, Florida.

Lin, C.-C. and Mignolet, M. P., 1997, "An Adaptive Perturbation Scheme for the Analysis of Mistuned Bladed Disks," *ASME Journal of Engineering for Gas Turbines and Power*, Vol. 119, No. 1, pp. 153–160.

Menq, C.-H., Griffin, J. H., and Bielak, J., 1986, "The Forced Response of Shrouded Fan Stages," *ASME Journal of Vibration, Acoustics, Stress, and Reliability in Design*, Vol. 108, pp. 50–55.

Mignolet, M. P. and Lin, C.-C., 1997, "Identification of Structural Parameters in Mistuned Bladed Disks," *ASME Journal of Vibration and Acoustics*, Vol. 119, No. 3, pp. 428–438.

Pierre, C., 1988, "Mode Localization and Eigenvalue Loci Veering Phenomena in Disordered Structures," *Journal of Sound and Vibration*, Vol. 126, No. 3, pp. 485–502.

Srinivasan, A. V., 1997, "Flutter and Resonant Vibration Characteristics of Engine Blades," *ASME Journal of Engineering for Gas Turbines and Power*, Vol. 119, No. 4, pp. 742–775.

Srinivasan, A. V., Lionberger, S. R., and Brown, K. W., 1978, "Dynamic Analysis of an Assembly of Shrouded Blades Using Component Modes," *ASME Journal of Mechanical Design*, Vol. 100, pp. 520–527.

Strang, G., 1988, *"Linear Algebra and Its Applications"*, Saunders HBJ, third edition.

Thomas, D. L., 1979, "Dynamics of Rotationally Periodic Structures," *International Journal for Numerical Methods in Engineering*, Vol. 14, pp. 81–102.

Valero, N. A. and Bendiksen, O. O., 1986, "Vibration Characteristics of Mistuned Shrouded Blade Assemblies," *ASME Journal of Engineering for Gas Turbines and Power*, Vol. 108, pp. 293–299.

Wagner, J. T., 1967, "Coupling of Turbomachine Blade Vibrations Through the Rotor," *ASME Journal of Engineering for Power*, Vol. 89, No. 4, pp. 502–512.

Wei, S. T. and Pierre, C., 1988a, "Localization Phenomena in Mistuned Assemblies with Cyclic Symmetry, Part I: Free Vibrations," *ASME Journal of Vibration, Acoustics, Stress, and Reliability in Design*, Vol. 110, No. 4, pp. 429–438.

Wei, S. T. and Pierre, C., 1988b, "Localization Phenomena in Mistuned Assemblies with Cyclic Symmetry, Part II: Forced Vibrations," *ASME Journal of Vibration, Acoustics, Stress, and Reliability in Design*, Vol. 110, No. 4, pp. 439–449.

Yang, M.-T. and Griffin, J. H., 1997, "A Reduced Order Approach for the Vibration of Mistuned Bladed Disk Assemblies," *ASME Journal of Engineering for Gas Turbines and Power*, Vol. 119, pp. 161–167.

Zheng, Z.-c. and Wang, F.-r., 1985, "Dynamic Analysis of Blade Groups Using Component Mode Synthesis," in *Vibrations of Blades and Bladed Disk Assemblies, Proceedings of the ASME 10th Biennial Conference on Mechanical Vibration and Noise,* Cincinnati, Ohio, pp. 97–103.

APPENDIX A: THE KRONECKER PRODUCT

The Kronecker product of two matrices is defined as:

$$\mathbf{A}\otimes\mathbf{B}=\begin{bmatrix} a_{11}\mathbf{B} & a_{12}\mathbf{B} & \dots & a_{1N}\mathbf{B} \\ a_{21}\mathbf{B} & a_{22}\mathbf{B} & \dots & a_{2N}\mathbf{B} \\ \vdots & \vdots & \ddots & \vdots \\ a_{N1}\mathbf{B} & a_{N2}\mathbf{B} & \dots & a_{NN}\mathbf{B} \end{bmatrix} \tag{A.1}$$

Selected useful properties of the Kronecker product:

$$(\mathbf{A}\otimes\mathbf{B})(\mathbf{C}\otimes\mathbf{D})=(\mathbf{AC})\otimes(\mathbf{BD}) \tag{A.2}$$

$$(\mathbf{A}\otimes\mathbf{B})^{-1}=\mathbf{A}^{-1}\otimes\mathbf{B}^{-1} \tag{A.3}$$

$$(\mathbf{A}\otimes\mathbf{B})^{\mathbf{T}}=\mathbf{A}^{\mathbf{T}}\otimes\mathbf{B}^{\mathbf{T}} \tag{A.4}$$

APPENDIX B: CIRCULANT MATRICES / CYCLIC SYMMETRY

The reduced order model formulation outlined in this paper makes frequent use of the properties of circulant matrices and their eigenvectors, as applied to cyclic symmetry problems. The properties of circulant matrices are thoroughly examined in Davis (1979). Moreover, a detailed description of modes of vibration for cyclic structures is contained in the important work by Thomas (1979), although certain related mathematical aspects, such as the fundamentals of circulant matrices, appear to have been unrealized at the time.

The general form of a square circulant matrix is:

$$\mathbf{C}=\mathbf{circ}\,(c_1,c_2,\dots,c_N)=\begin{bmatrix} c_1 & c_2 & \dots & c_N \\ c_N & c_1 & \dots & c_{N-1} \\ \vdots & \vdots & \ddots & \vdots \\ c_2 & c_3 & \dots & c_1 \end{bmatrix} \tag{B.1}$$

All circulant matrices of order N possess N independent eigenvectors. In particular, they share the same set of eigenvectors that make up the complex Fourier matrix, $\mathbf{E}$:

$$\mathbf{E}=[e_{ki}]\;;\quad e_{ki}=\tfrac{1}{\sqrt{N}}e^{j\alpha(i-1)(k-1)}\qquad k,i=1,\dots,N \tag{B.2}$$

where $j=\sqrt{-1}$, and $\alpha=2\pi/N$. In addition, there exists an "almost-equivalent" real-valued form of Eq. (B.2):

$$\mathbf{F}=\begin{bmatrix}\mathbf{f_0} & \mathbf{f_{1,c}} & \mathbf{f_{1,s}} & \cdots & \mathbf{f_{n,c}} & \mathbf{f_{n,s}} & \cdots & \mathbf{f_{N/2}}\end{bmatrix}= \tag{B.3}$$

$$\begin{bmatrix} \frac{1}{\sqrt{N}} & \sqrt{\frac{2}{N}} & 0 & \cdots & \frac{1}{\sqrt{N}} \\ \frac{1}{\sqrt{N}} & \sqrt{\frac{2}{N}}\cos\alpha & \sqrt{\frac{2}{N}}\sin\alpha & \cdots & -\frac{1}{\sqrt{N}} \\ \frac{1}{\sqrt{N}} & \sqrt{\frac{2}{N}}\cos 2\alpha & \sqrt{\frac{2}{N}}\sin 2\alpha & \cdots & \frac{1}{\sqrt{N}} \\ \vdots & \vdots & \vdots & & \vdots \\ \frac{1}{\sqrt{N}} & \sqrt{\frac{2}{N}}\cos(N-1)\alpha & \sqrt{\frac{2}{N}}\sin(N-1)\alpha & \cdots & \frac{(-1)^{N-1}}{\sqrt{N}} \end{bmatrix}$$

where the last column only exists if N is even.

Note that both $\mathbf{E}$ and $\mathbf{F}$ are *orthonormal*, or *unitary*, such that $\mathbf{E}^*\mathbf{E}=\mathbf{F}^{\mathbf{T}}\mathbf{F}=\mathbf{I}$, where $\mathbf{I}$ is an identity matrix of size N, and $*$ denotes the Hermitian adjoint (complex conjugate transpose). In addition, this implies that $\mathbf{E}^{-1}=\mathbf{E}^*$ and $\mathbf{F}^{-1}=\mathbf{F}^{\mathbf{T}}$, such that the typical transformation products $\mathbf{E}^*\mathbf{CE}$ and $\mathbf{F}^{\mathbf{T}}\mathbf{CF}$ are *similarity transformations* (Strang, 1988).

The reason behind calling $\mathbf{F}$ "almost-equivalent" to $\mathbf{E}$ is that the columns of $\mathbf{F}$ are not true eigenvectors of $\mathbf{C}$, and hence, the similarity transformation $\mathbf{F}^{\mathbf{T}}\mathbf{CF}$ will not yield a diagonalized matrix. However, it will result in a matrix where all non-zero elements will be grouped into 2×2 blocks ("double" harmonics) on the diagonal, except for the $(1,1)$ and, for N even, the (N,N) elements ("single" harmonics). This matrix type is referred to as *pseudo-block-diagonal.*

These properties are readily extended to the case of *block-circulant* matrices by expanding $\mathbf{E}$ and $\mathbf{F}$ as $\mathbf{E}\otimes\mathbf{I}$ and $\mathbf{F}\otimes\mathbf{I}$, respectively. The scalar c_i then represents a matrix block $\mathbf{C_i}$, where $\mathbf{C_i}$ and $\mathbf{I}$ are of the same size. The symbol $\otimes$ denotes the Kronecker product, which is defined in Appendix A.

From the theory of symmetrical components, one may relate some quantity $\mathbf{x_n}$ (i.e., displacements, forces, etc.) in physical coordinates for the nth sector to the corresponding quantity $\mathbf{u^k}$ in cyclic coordinates for a fundamental sector by:

$$\mathbf{x}=(\mathbf{F}\otimes\mathbf{I})\,\mathbf{u} \tag{B.4}$$

where:

$$\mathbf{x}=\begin{Bmatrix}\mathbf{x_1}\\ \mathbf{x_2}\\ \mathbf{x_3}\\ \vdots\\ \mathbf{x_N}\end{Bmatrix}\qquad \mathbf{u}=\begin{Bmatrix}\mathbf{u^0}\\ \mathbf{u^{1c}}\\ \mathbf{u^{1s}}\\ \mathbf{u^{2c}}\\ \vdots\\ \mathbf{u^{N/2}}\end{Bmatrix} \tag{B.5}$$

$\mathbf{I}$ has the size of the number of elements in $\mathbf{u^k}$, and $\mathbf{F}$ is defined in Eq. (B.3). In the context of this work, the quantities $\mathbf{x}$ and $\mathbf{u}$ represent nodal displacements in physical and cyclic coordinates, respectively.

A structure that exhibits cyclic symmetry will have structural matrices (mass and stiffness) that may be represented in block-circulant form. Thus, in structural analyses of cyclic structures, the pseudo-block-diagonalization achieved via the coordinate transformation in Eq. (B.4) leads to significant problem size reduction and hence, substantial improvement in computational efficiency. Note that a similar degree of problem size reduction may be obtained using a complex approach, by employing the Fourier matrix, $\mathbf{E}$, defined in Eq. (B.2).